IEEE Open Access Journal of
Power and Energy

Received 16 September 2022; revised 17 January 2023; accepted 30 January 2023. Date of publication 13 February 2023;
date of current version 24 May 2023.

Digital Object Identifier 10.1109/OAJPE.2023.3244330

A New Analytical Model of Single-Phase Diode Bridge Rectifiers in the Presence of Interharmonics in Supply Voltage

JIRI DRAPELA[1] (Senior Member, IEEE), ROBERTO LANGELLA[2] (Senior Member, IEEE), ALFREDO TESTA[2] (Life Fellow, IEEE), AND VINCENZO VENDEMIA[3]

[1]Department of Electrical Power Engineering, Faculty of Electrical Engineering and Communication, Brno University of Technology, 601 90 Brno, Czech Republic
[2]Department of Engineering, University of Campania "Luigi Vanvitelli," 81031 Aversa, Italy
[3]NIDEC ASI S.P.A., 20092 Cinisello Balsamo, Italy

CORRESPONDING AUTHOR: R. LANGELLA (roberto.langella@unicampania.it)

This work was supported in part by the Centre for Research and Utilization of Renewable Energy, and in part by the Ministry of Education, Youth and Sports of the Czech Republic under Brno University of Technology Specific Research Program under Project FEKT-S-23-8403.

ABSTRACT In this paper, a new accurate and comprehensive analytical model of harmonic and interharmonic distortion produced by a single-phase AC/DC diode bridge rectifier (DBR) is presented. Its main and new characteristic is the ability to consider the presence of interharmonics in addition to harmonics in the voltage at the terminals of DBR due to the background distortion. Analytical expressions able to predict DC voltage and AC current either in time or frequency domains are obtained. Several numerical and experimental tests have been performed showing very accurate results. The proposed model presents all the advantages of analytical models (e.g., fastness); therefore, it can be easily integrated with iterative harmonic and interharmonic analysis procedures. Subsequent applications are the possibility to perform parametric analyses and probabilistic studies, to derive harmonically and interharmonically coupled admittance matrices, to help in introducing standard limits for interharmonics.

INDEX TERMS Analytical model, harmonics, interharmonics, power quality, single phase rectifiers.

I. INTRODUCTION

HARMONIC distortion of electronic equipment fed by single-phase diode rectifiers with smoothing capacitor has been widely studied since the beginning of nineties developing very accurate analytical models [1], [2], [3], [4], [5], [6], [7], [8], [9], [10], [11], [12], [13]. Recently in [14] the harmonically coupled admittance matrix of the single-phase DBR was analytically derived to solve convergence problems of the iterative harmonic analysis (IHA) of networks with nonlinear loads. These models can consider accurately the presence of background (BG) harmonic distortion in the supply voltage (i.e., the pre-existing voltage applied to the terminals of the equipment before its connection), but they are not capable to cope with BG voltage interharmonics.

Interharmonics are spectral components at frequencies that are not integer multiple of the system fundamental frequency [15]; as such they can significantly affect the response of nonlinear loads, especially DBRs. In future distribution networks, increased levels of BG voltage interharmonics due to the increased number of equipment emitting interharmonic currents are expected. It is in fact well known that some distributed generation devices (PV generating units), high efficiency industrial systems (Variable Speed Drives, commercial Heat Ventilation Air Conditioning Systems) and residential equipment (inverter air conditioning, washing machines, refrigerators, ...) produce interharmonic currents due to their inherent time varying nature [16], [17], [18], [19], [20], [21], [22], [23], [24], [25].

For these reasons, interharmonics limits are subject of discussion in the standardization community [26] and [27]. The new edition of the IEEE Standard 519 [27] contains the Appendix A where the rationale for low voltage interharmonic limits of non-generation installations is discussed but without specific limits as there is not enough knowledge on this topic.

The presence of interharmonics has the ability of changing the periodicity of the signals which are no longer periodical of the system fundamental period. In [16] the concept of Fourier fundamental angular frequency, ω_F, which is the Greatest Common Divisor of all the frequency components contained into the signal, has been introduced. It was also demonstrated that the introduction of a new base frequency (e.g., the Fourier fundamental frequency, f_F) allows transforming the problem of modeling harmonics and interharmonics of the system frequency (50 or 60 Hz) into that of modeling harmonics of the base frequency (e.g., 5 Hz). This allows, in principle, to adopt each kind of technique proposed for harmonic penetration studies, also in the presence of interharmonics. In [16] the concept of Fourier fundamental frequency was used to include interharmonics in either steady state or dynamic modified domains.

This paper builds on the initial results and analysis presented in [28], where the analytical model of harmonic and interharmonic distortion produced by a single-phase DBR was firstly presented. The main and new characteristic of the model is the ability to consider the presence of interharmonics in addition to harmonics in the voltage at the terminals of the DBR due to the background distorted voltage. Here, analytical expressions able to predict DC voltage and AC current in frequency domain, further on the solution in time domain presented in [28], are proposed. Moreover, the results of several numerical and experimental tests are reported here, showing very accurate results. The proposed model presents all the advantages of analytical models (e.g., fastness); therefore, it can be easily integrated with iterative harmonic and interharmonic analysis procedures. Subsequent applications are the possibility to perform parametric analyses and probabilistic studies, to derive harmonically and interharmonically coupled admittance matrices to be included in harmonic and interharmonic power flow studies, to have a more direct insight in the physical behavior of the devices helping in introducing standard limits for interharmonics.

The reminder of the paper is: Section II contains the model description; Section III reports the analytical solution both in time and frequency domains; Section IV analyses the results of numerical and experimental validation and, finally, Section V contains the conclusions of the paper.

II. MODEL DESCRIPTION

A. CIRCUIT DESCRIPTION

Fig. 1 shows a simplified equivalent circuit of a typical single-phase DBR interfaced nonlinear equipment. Its power supply stage relevant for AC input current waveform in power frequency range is formed by a DBR feeding a DC-to-DC block modeled by means of an equivalent resistance [6]. The voltage generator v models a distorted supply voltage which includes BG harmonics and interharmonics. Passive components $R_L, R_C, L_L,$ and L_C are equivalent resistances and inductances, such as those (in generalized scheme) present at AC and DC sides of the DBR (e.g., R_L includes supply equivalent resistance, wire resistance, diode resistance and the device input resistor resistance); C is a bulk DC-smoothing capacitor. The capacitor may feed a DC-to-DC stage, which converts input DC voltage, v_c, into a regulated DC voltage, and is generally modeled as an equivalent resistor R_D. The hypothesis regarding suitability of the equivalent load R_D for low-frequency response modelling has been confirmed experimentally in [29] and in [30].

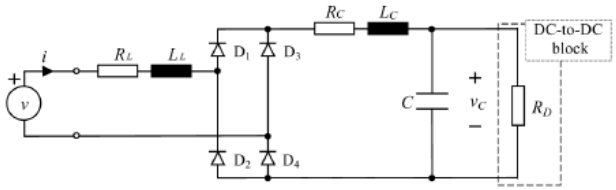

FIGURE 1. **Single-phase uncontrolled rectifier circuit.**

B. PROBLEM STATEMENT

Let's consider a distorted voltage normalized to rated RMS value:

$$\begin{aligned} v_N(t) &= v_{N,1}(t) + \sum_{h\in S_h} v_{N,h}(t) + \sum_{ih\in S_{ih}} v_{N,ih}(t) \\ &= \sqrt{2}V_{N,1}\cos(\omega_1 t + \phi_1) + \sum_{h\in S_h} \sqrt{2}V_{N,h}\cos(\omega_h t + \phi_h) \\ &\quad + \sum_{ih\in S_{ih}} \sqrt{2}V_{N,ih}\cos(\omega_{ih} t + \phi_{ih}), \end{aligned} \tag{1}$$

where: $v_{N,1}$, $v_{N,h}$ and $v_{N,ih}$ are, respectively, the normalized fundamental, harmonics and interharmonic time waveforms of the AC supply voltage; $V_{N,1}$, $V_{N,h}$, $V_{N,ih}$, ω_1, ω_h, ω_{ih} and $\phi_1, \phi_h, \phi_{ih}$ are the normalized rms values, angular frequencies and the initial phase angles of the fundamental, harmonics and interharmonics of the voltage; S_h and S_{ih} are the sets of harmonic and interharmonic indices.

Introducing the concept of Fourier fundamental angular frequency, ω_F, (1) can be rewritten in this way:

$$v_N(\theta) = \sum_{k=1}^{K} \sqrt{2}V_{N,k}\cos(k\theta_F + \phi_k), \tag{2}$$

where θ is the instantaneous phase angle, $\theta_F = \omega_F \cdot t$, $V_{N,k}$ and ϕ_k are the normalized rms value and the initial phase angle, respectively, of the $k-$th harmonic component of ω_F, K is the maximum number of frequency components considered, $K = \omega_{MAX} \,/\, \omega_F$. All the components in (2) are harmonics of the ω_F, those components of order k integer multiple of $\omega_1 \,/\, \omega_F$ are also harmonics of the system fundamental angular frequency ω_1, while the other components are interharmonics.

All of the models for harmonic studies present in literature ([1], [2], [3], [4], [5], [6], [7], [8], [9], [10], [11], [12], [13], [14]) are based on the following basic assumption: the AC-voltage network is affected by BG odd harmonics only, that is to say, there is a symmetry between the positive half-cycle and negative half-cycle of the fundamental period.

This assumption is no more valid in the presence of interharmonics. Fig. 2 shows, for illustration purposes, the results

of an experimental test performed in laboratory where a DBR with an RC load (according to the Fig. 1) was fed by an interharmonic voltage of $V_{N,ih} = 1$ % of base voltage V_1 with a frequency $f_{ih} = 425$ Hz superimposed to the 50 Hz (see details about test setup and measurements in section IV-A). The shown quantities are the waveforms of the normalized AC supplying voltage, v_N, the DC-link voltage $v_{C,N}$, and the AC absorbed current, i_N, normalized by the base current V_1/R_D being R_D the base resistance. The interharmonic component frequency of 425 Hz was chosen so that the combined supply voltage period is only 40 ms, that is two times that of the fundamental. Consequently, the Fourier fundamental frequency is 25 Hz (i.e., the Greater Common Divisor between 50 Hz, the system fundamental frequency, and 425 Hz, the interharmonic component frequency), so two Fourier fundamental periods are plotted for all the quantities: voltages and current repeat themselves two times. It is evident that the asymmetry between each consecutive half period of the system fundamental frequency is confirmed.

For each period of the Fourier fundamental frequency a sequence of subintervals, $\Theta^{(j)}$, with $j = 1, \ldots, J$, can be considered. In each subinterval two modes can be distinguished:

i) "charging mode" where the current flows in the DBR, charges the bulk capacitor and feeds the DC load directly, and

ii) "discharging mode" where no current flows from the supply and the capacitor feeds the DC load.

It can be concluded that in the presence of BG interharmonics in the supplying voltage: 1) it is necessary to refer to the Fourier fundamental period; 2) it is not possible to apply all the simplifying assumptions of waveform symmetry that are used when only odd harmonics are present in the BG voltage; and 3) it can no longer be assumed that there are only odd harmonics in the AC current and only even harmonics in DC voltage.

C. MATHEMATICAL MODEL

For each subinterval, $\Theta^{(j)}$, three commutation angles can be defined (see Fig. 2): $\theta_1^{(j)}$ and $\theta_2^{(j)}$ which represent the beginning and the end of the conduction of the rectifier and $\theta_3^{(j)}$ which represents the end of the DC capacitor discharge. Obviously, $\theta_3^{(j)} = \theta_1^{(j+1)}$.

It is possible to write the following system of differential equations which allows to evaluate the waveforms of the current absorbed by the rectifier as well as of the voltage across its DC-smoothing capacitor:

$$\begin{cases} i_N^{(j)}(\theta) = 0, & \theta_2^{(j)} \leqslant \theta < \theta_3^{(j)} \\ \dfrac{1}{x_{C,N}} \dfrac{dv_{C,N}^{(j)}}{d\theta} + v_{C,N}^{(j)}(\theta) = 0, & \theta_2^{(j)} \leqslant \theta < \theta_3^{(j)} \\ x_{L,N} \dfrac{di_N^{(j)}}{d\theta} + r_N \cdot i_N^{(j)}(\theta) + q \cdot v_{C,N}^{(j)}(\theta) = v_N(\theta), & \theta_1^{(j)} \leqslant \theta < \theta_2^{(j)} \\ \dfrac{1}{x_{C,N}} \dfrac{dv_{C,N}^{(j)}}{d\theta} + v_{C,N}^{(j)}(\theta) = q \cdot i_N^{(j)}(\theta), & \theta_1^{(j)} \leqslant \theta < \theta_2^{(j)} \end{cases} \tag{3}$$

where the circuit voltages, currents and impedances are normalized as in [10]:

$$\begin{aligned} r_N = \frac{R_L + R_C}{R_D},\ x_{L,N} = \frac{X_L}{R_D},\ x_{C,N} = \frac{X_C}{R_D}, \\ X_L = \omega_F \cdot (L_L + L_C)\ ,\ X_C = 1/(\omega_F \cdot C), \end{aligned} \tag{4}$$

and being q equal to $+1$ (-1) if $v_N(\theta) \geq 0 (v_N(\theta) < 0)$.

The respective segment change conditions are:

$$\begin{cases} i_N^{(j)}(\theta_2^{(j)}) = 0, \\ v_{C,N}^{(j)}(\theta_1^{(j)}) = \mathrm{q} \cdot v_N^{(j)}(\theta_1^{(j)}), \\ v_{C,N}^{(j)}(\theta_3^{(j)}) = v_{C,N}^{(j)}(\theta_1^{(j+1)}), \\ i_N^{(j)}(\theta_3^{(j)}) = i_N^{(j)}(\theta_1^{(j+1)}) = 0. \end{cases} \tag{5}$$

III. ANALYTICAL SOLUTION

In this section the solutions of the system (3) both in time and frequency domains under the segment change conditions (5) together with the algorithm for the estimation of the commutation instants of the DBR are reported.

A. TIME DOMAIN SOLUTION

For each subinterval, $\Theta^{(j)}$, the time analytical expressions of the normalized AC absorbed current and DC-link voltage are calculated solving (3), under the conditions (5), by Laplace transform. Their compact expressions are as in (6), shown at the bottom of the next page, where s_1, s_2, β_3, $C_k^{(j,i)}$ and $G_k^{(j,i)}$ (i=1 to 4 for $C_k^{(j,i)}$ and i=0 to 4 for $G_k^{(j,i)}$) are constants whose analytical expressions are reported in Appendix A.

It is possible to observe that being the boundary conditions different for each of the J different subintervals, J different solutions over the Fourier fundamental period must be calculated individually with its own sets of commutation angles as shown in the following subsection.

For a whole periodicity interval ($2\pi/\omega_F$), due to the independence of each $j-$th subinterval, the following final expressions of AC current and DC voltage can be written:

$$\begin{cases} i_N(\theta) = \sum_{j=1}^{J} i_N^{(j)}(\theta)\,, \\ v_{C,N}(\theta) = \sum_{j=1}^{J} v_{C,N}^{(j)}(\theta). \end{cases} \quad \text{with } 0 \leq \theta < 2\pi. \tag{7}$$

B. COMMUTATION ANGLES ESTIMATION

The calculation of the commutation angles is performed under the hypothesis that the voltage on the DBR is equal to the supply voltage (neglecting the voltage drop across the input impedance), as commonly done in the scientific literature on this topic with reference to harmonics.

The iterative procedure for the angles calculation is reported in the flow-chart shown in Fig. 3 and is based on Gauss-Seidel approach as in [5] but Newton based methods can also be used.

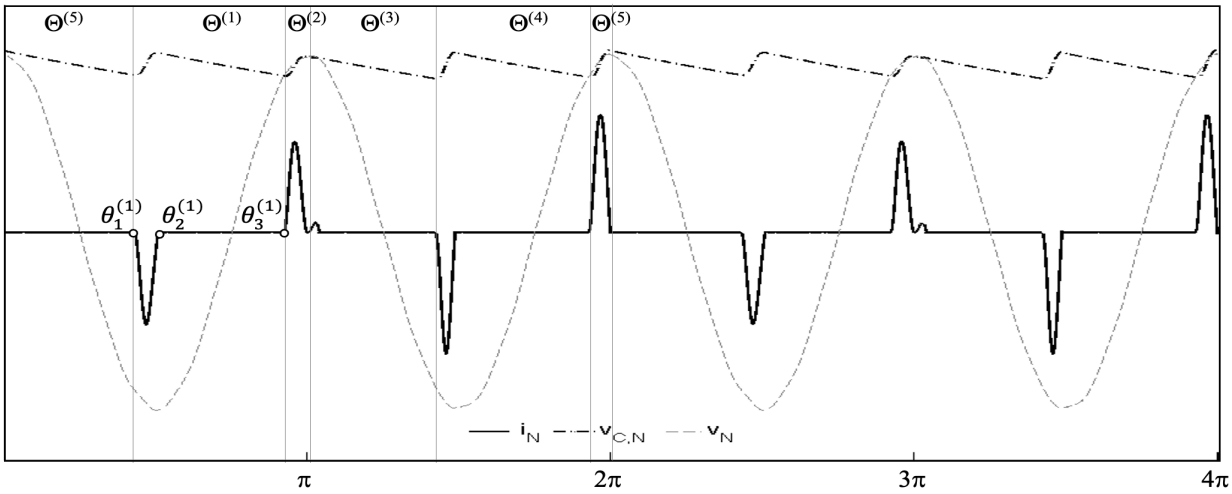

FIGURE 2. Laboratory test: normalized AC supplying voltage, v_N, AC absorbed current, i_N, and DC-link voltage v_{CN} waveforms when an interharmonic voltage of 1%@425 Hz was superimposed to the system fundamental voltage @50 Hz.

The equations to solve during each iteration are:

$$i_N^{(j)}(\theta_2^{(j)}) = 0 \tag{8}$$

$$v_{C,N}^{(j)}(\theta_3^{(j)}) = \mathrm{q} \cdot v_N^{(j)}(\theta_3^{(j)}). \tag{9}$$

The iterative procedure consists of the following steps (starting from j=1):

a) Assume a starting angle $\underline{\theta}_1^{(1)}$(e.g., $\underline{\theta}_1^{(1)}$=0).
b) Impose $\theta_1^{(1)}$=$\underline{\theta}_1^{(1)}$.
c) Solve (8) for $\theta_2^{(j)}$ using the expression of $i_N^{(j)}$ for $\theta_1^{(1)} \leq \theta < \theta_2^{(j)}$ in the first equation in (6).
d) Using $\theta_2^{(j)}$, solve (9) for $\theta_3^{(j)}$ using the expression of $v_{C,N}^{(j)}(\theta)$ for $\theta_2^{(1)} \leq \theta < \theta_3^{(j)}$ in the second equation in (6).
e) If $\theta_3^{(j)} < 2\pi$, impose j=$j+1$ and $\theta_1^{(j)} = \theta_3^{(j-1)}$.
f) Repeat the steps c) and d) until $\theta_3^{(j)} \leq 2\pi$.
g) If $\theta_3^{(j)} \geq 2\pi$ assume $\theta_1^{(1)} = \theta_3^{(j)} - 2\pi$.
h) Evaluate the error between previous and following step through $\theta_1^{(1)}$- $\underline{\theta}_1^{(1)}$ and if the absolute value of this difference is lower than an assigned error ε or equal, the procedure ends.
i) If $|\theta_1^{(1)}$- $\underline{\theta}_1^{(1)}| > \varepsilon$, all steps from c) are repeated until h) is true.

C. FREQUENCY DOMAIN SOLUTION

For each subinterval, $\Theta^{(j)}$, the frequency spectral components of the AC currents and DC voltage, respectively, can be obtained introducing the following terms:

$$\underline{I}_{N,h}^{(j,1)},\ \underline{I}_{N,h}^{(j,2)},\ \underline{I}_{N,h}^{(j,3)},\ \underline{I}_{N,h}^{(j,4)},$$

and

$$\underline{V}_{C,N,m}^{(j,0)},\ \underline{V}_{C,N,m}^{(j,1)},\ \underline{V}_{C,N,m}^{(j,2)},\ \underline{V}_{C,N,m}^{(j,3)},\ \underline{V}_{C,N,m}^{(j,4)},$$

$$\begin{cases} \begin{pmatrix} i_N^{(j)}(\theta) \\ v_{C,N}^{(j)}(\theta) \end{pmatrix} = \sum_{k=1}^{K} \sqrt{2} V_{N,k} \left[\begin{pmatrix} C_k^{(j,1)} \\ G_k^{(j,1)} \end{pmatrix} e^{s_1(\theta-\theta_1^{(j)})} + \begin{pmatrix} C_k^{(j,2)} \\ G_k^{(j,2)} \end{pmatrix} e^{s_2(\theta-\theta_1^{(j)})} \right. \\ \qquad + \begin{pmatrix} C_k^{(j,3)} \\ G_k^{(j,3)} \end{pmatrix} \cos(k(\theta-\theta_1^{(j)})) \\ \qquad \left. + \begin{pmatrix} C_k^{(j,4)} \\ G_k^{(j,4)} \end{pmatrix} \sin(k(\theta-\theta_1^{(j)})) \right], \ \theta_1^{(j)} \leqslant \theta < \theta_2^{(j)} \\ \begin{pmatrix} i_N^{(j)}(\theta) \\ v_{C,N}^{(j)}(\theta) \end{pmatrix} = \begin{bmatrix} 0 \\ \left(\sum_{k=1}^{K} \sqrt{2} V_{N,k} G_k^{(j,0)} \right) e^{-\beta_3(\theta-\theta_2^{(j)})} \end{bmatrix}, \ \theta_2^{(j)} \leq \theta < \theta_3^{(j)} \\ \begin{pmatrix} i_N^{(j)}(\theta) \\ v_{C,N}^{(j)}(\theta) \end{pmatrix} = \begin{pmatrix} 0 \\ 0 \end{pmatrix}, \ 0 \leqslant \theta < \theta_1^{(j)} \text{ and } \theta_3^{(j)} \leq \theta < 2\pi \end{cases} \tag{6}$$

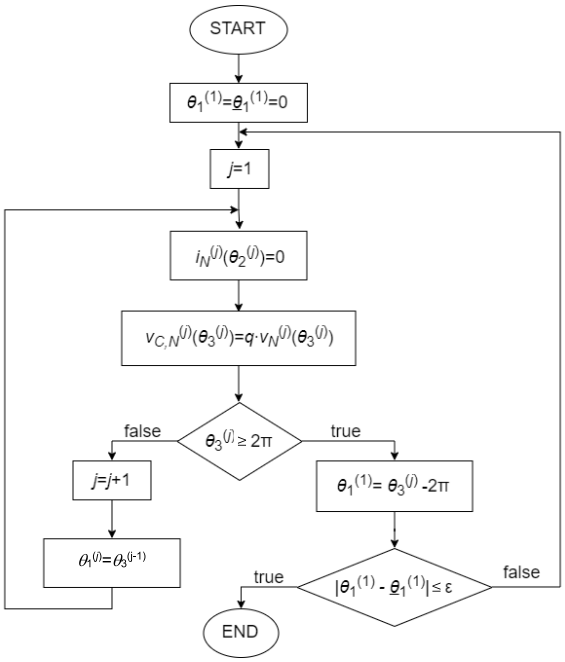

FIGURE 3. **Iterative procedure to calculate the conduction angles.**

whose analytical expressions are obtained analytically applying the complex Fourier series to each corresponding term in the expression (6) as reported in Appendix B.

For a whole periodicity interval due to the independence of each $j-$th subinterval, the following final expressions of AC current and DC voltage phasors (with $h = 0, 1, 2, 3, \ldots$ and $m = 0, 1, 2, \ldots$) are:

$$\begin{cases} \underline{I}_{N,h} = \sum_{j=1}^{J} \left(\underline{I}_{N,h}^{(j,1)} + \underline{I}_{N,h}^{(j,2)} + \underline{I}_{N,h}^{(j,3)} + \underline{I}_{N,h}^{(j,4)} \right), \\ \underline{V}_{C,N,m} = \sum_{j=1}^{J} \left(\underline{V}_{C,N,m}^{(j,0)} + \underline{V}_{C,N,m}^{(j,1)} + \underline{V}_{C,N,m}^{(j,2)} \right. \\ \qquad \left. + \underline{V}_{C,N,m}^{(j,3)} + \underline{V}_{C,N,m}^{(j,4)} \right). \end{cases} \tag{10}$$

IV. NUMERICAL AND EXPERIMENTAL VALIDATION

Several laboratory tests were performed, varying the amplitude and frequency of the BG supply voltage interharmonics, system parameters and considering different types of DBR based loads. For each experimental test a numerical model implemented in Simulink environment according to the equivalent scheme of Fig. 1 was derived to also have a numerical reference to test the accuracy performances of the proposed analytical model.

A. LABORATORY SETUP

The supply voltage source was simulated employing a 5 kVA AC programmable power source by California Instruments (model CI 5000iX). Actual supply system line (source) impedance was kept as small as possible. An equivalent modular impedance network, consisting of multiple modules, $\underline{Z}_m$, in series connection, was connected between the power source and the load under test to also control (emulate) the value of the longitudinal mains impedance. The single module impedance is 0.59 + j0.34 Ω at 50 Hz. In relation to Fig. 1, the physical modular impedance network is then included in R_L an L_L. Power supply fundamental voltage was set to 230V@50Hz with a superimposed single interharmonic component with individual frequency and magnitude for each test.

Measurements to capture waveforms were performed using a multi-channel precision power analyzer (model LMG500) fully remotely controlled from a PC. The load input AC terminal and DC bus voltages on tested loads were sensed directly by the LMG500 voltage inputs while the AC absorbed current was measured using direct current input of the LMG500 instrument. Measured signals spectral component frequencies required to derive the Fourier fundamental frequency for subsequent analysis are predicted from known supply voltage components (see Table 1 again).

B. TEST SCENARIOS

Three different experimental scenarios were considered. In test scenario 1: a "didactic" physical model (representable by the scheme of Fig. 1) consisting of a single-phase DBR feeding a bulk capacitor and a variable output resistor was used. The load was connected to the power source via 3 $\underline{Z}_m$, in tests from 1.1 to 1.6 and 1 $\underline{Z}_m$ in tests from 1.7 to 1.12.

TABLE 1. **Details about all the performed experimental tests with $\underline{Z}_m$ = (0.59 + j0.34) Ω.**

Test No.	f_{ih} (Hz)	$V_{N,ih}$ (%)	Supply imped.	Load type	R_L (Ω)	L_L (mH)	C (μF)	R_D (kΩ)
1.1	25	1	3 $\underline{Z}_m$	DBR	4	3.55	24.8	1.132
1.2	25	10	3 $\underline{Z}_m$	DBR	4	3.55	24.8	1.132
1.3	225	1	3 $\underline{Z}_m$	DBR	4	3.55	24.8	1.132
1.4	225	10	3 $\underline{Z}_m$	DBR	4	3.55	24.8	1.132
1.5	425	1	3 $\underline{Z}_m$	DBR	4	3.55	24.8	1.132
1.6	425	5	3 $\underline{Z}_m$	DBR	4	3.55	24.8	1.132
1.7	25	1	1 $\underline{Z}_m$	DBR	2	1.25	53.8	1.132
1.8	25	10	1 $\underline{Z}_m$	DBR	2	1.25	53.8	1.132
1.9	225	1	1 $\underline{Z}_m$	DBR	2	1.25	53.8	1.132
1.10	225	10	1 $\underline{Z}_m$	DBR	2	1.25	53.8	1.132
1.11	425	1	1 $\underline{Z}_m$	DBR	2	1.25	53.8	1.132
1.12	425	5	1 $\underline{Z}_m$	DBR	2	1.25	53.8	1.132
2.1	175	10	1 $\underline{Z}_m$	CFL	12	2.4	9.6	4.400
2.2	283	5	1 $\underline{Z}_m$	CFL	12	2.4	9.6	4.400
2.3	283	5	0 $\underline{Z}_m$	CFL	11	1.4	9.6	4.400
3.1	**175**	**10**	1 $\underline{Z}_m$	**LED**	**31**	**1.8**	**2.95**	**7.400**
3.2	283	5	1 $\underline{Z}_m$	LED	31	1.8	2.95	7.400

In test scenario 2: a compact fluorescent lamp (CFL) (Osram DULUX EL 23W/21-827 E27) was tested with 1 $\underline{Z}_m$ and with 0 $\underline{Z}_m$ (Supply impedance →0 in Table 1). Its scheme can be equivalently simplified through a full-wave DBR loaded by a bulk capacitor and a resistor representing the equivalent lamp connected in parallel [29], [30], [31].

TABLE 2. Test 3.1 (LED) Convergence of the iterative procedure for the commutation angles in Rad.

$\Theta^{(1)}$		$\Theta^{(2)}$		$\Theta^{(3)}$		$\Theta^{(4)}$	
$\theta_1^{(1)}$	$\theta_2^{(1)}$	$\theta_1^{(2)}$	$\theta_2^{(2)}$	$\theta_1^{(3)}$	$\theta_2^{(3)}$	$\theta_1^{(4)}$	$\theta_2^{(4)}$
0	0.219	1.270	1.675	2.801	3.126	4.300	4.631
-0.451	0.219	1.270	1.675	2.801	3.126	4.300	4.631
-0.451	0.219	1.270	1.675	2.801	3.126	4.300	4.631

In test scenario 3: a light-emitting diode (LED) lamp (Panasonic LDAHV10L27CGE 10W 220-240 V) with 1 $\underline{Z}_m$. This equipment was demonstrated to be modellable with the simplified equivalent circuit of Fig. 1.

All the details of the test scenarios are summarized in Table 1 including the estimated parameters of the circuit in Fig. 1 (R_L, L_L, C and R_D while $R_C = 0\ \Omega$ and $L_C = 0$ H). The necessity to estimate the circuit parameters is due to the lack of this information for real loads. The numeric values of the circuit parameters have been estimated to minimize the mismatch between the simulated DC voltage and AC current and the corresponding measured wave-shapes using a root-mean-square deviation minimization procedure. It is important to note that the estimated set of the models' parameters accounts for all real circuit components' parameters (power source cubical wiring; leads; contacts; lamps' components, ...), including parasitic ones.

C. DETAILED RESULTS FOR ONE REPRESENTATIVE TEST

For the sake of brevity only detailed results for Test 3.1, highlighted with bold characters in Table 1, are reported while detailed results for the case 2.1 are reported in [28].

This test (as well as Tests 1.2, 1.4, 1.8, 1.10 and 2.1) corresponds to the practical (but extreme) situation that can happen when Ripple Control Signaling is used [31]. Fig. 4 shows the measured normalized waveforms of the supply voltage v_N, of the AC absorbed current i_N and of the DC-link voltage $v_{C,N}$; obtained from actual measurement (black solid), from the time domain analytical model of Subsection III-A (dash-dotted red), from the frequency domain analytical model of Subsection III-C (dashed blue) and from Simulink simulation (dotted green) for the entire Fourier period ($T_F = 40$ ms). It is possible to observe that the analytical model results match very well simulations and measurements. Moreover, it is evident that time and frequency domains analytical models give the same results, as expected.
Therefore, in what follows the ''proposed analytical model'' results are reported only once.

Table 2 reports the evolution of the commutation angles calculation obtained by means of the procedure described in Subsection III-B. It is possible to observe that the convergence is reached in only three steps.

Fig. 5 and Fig. 6 show the AC absorbed current harmonics and interharmonics, respectively, comparing those obtained from the proposed model, measurements, and simulations. Furthermore, percentage deviations between the results obtained by means of the proposed model (M), from measured (Mis) and simulated (Sim) results:

$$\varepsilon_{h,Mis}(\%) = \frac{|I_{h,M} - I_{h,Mis}|}{I_{h,Mis}} 100,\ \varepsilon_{\phi,Mis} = |\phi_{h,M} - \phi_{h,Mis}| \tag{11}$$

$$\varepsilon_{h,Sim}(\%) = \frac{|I_{h,M} - I_{h,Sim}|}{I_{h,Sim}} 100,\ \varepsilon_{\phi,Sim} = |\phi_{h,M} - \phi_{h,Sim}| \tag{12}$$

are reported upon the main frequency components.

From Fig. 5 and Fig. 6 it is possible to observe that the errors of the proposed method obtained assuming as reference the simulation results are much smaller (lower than 0.03%) than those assuming as reference the experimental results, as expected. In fact, the analytical model considers the same topology and uses the same component parameters as the Simulink model, whose equivalent circuit and parameters were derived starting from measurements on the real circuit.

Fig. 7 and Fig. 8 for the DC-link voltage harmonics and interharmonics, respectively, are equivalent to Fig. 5 and Fig. 6. For the sake of clarity, the DC components are removed from the graphics, but their amplitudes and corresponding errors are reported in the figure caption. Again, the results are very accurate.

TABLE 3. Total distortion percentage errors for AC current and DC voltage versus simulink simulations (Sim) and with actual measurements (Mis).

Test No.	SIM				MIS			
	AC current		DC voltage		AC current		DC voltage	
	ε_{THD}	ε_{TIHD}	ε_{THD}	ε_{TIHD}	ε_{THD}	ε_{TIHD}	ε_{THD}	ε_{TIHD}
1.1	0.03	0.02	0.01	0.08	-0.81	-0.62	0.94	-4.02
1.2	0.00	0.01	0.00	0.02	0.73	-0.43	1.83	-0.08
1.3	0.03	0.02	0.00	0.13	-0.82	-0.60	0.90	0.60
1.4	0.02	0.02	0.01	0.03	0.99	-0.28	2.43	-1.10
1.5	0.04	0.03	0.01	-0.01	-0.74	-0.52	1.09	4.42
1.6	0.02	0.02	0.01	-0.01	-0.91	-1.02	1.38	-3.10
1.7	0.03	0.03	0.01	-0.03	-1.19	-1.03	-1.68	-3.92
1.8	0.00	0.02	0.00	-0.01	-0.58	-1.13	-0.97	0.54
1.9	0.04	0.03	0.01	0.05	-1.23	-0.98	-1.88	-0.73
1.10	0.01	0.02	0.00	0.02	-1.57	-1.06	-1.27	-1.22
1.11	0.03	0.03	0.01	0.11	-1.15	-0.98	-1.63	-0.12
1.12	0.01	0.02	0.00	0.02	-0.44	-0.98	-1.05	-4.16
2.1	0.03	0.03	0.00	0.01	-0.40	1.40	0.72	-2.58
2.2	-0.19	-0.17	0.07	0.08	0.07	0.80	2.03	-1.66
2.3	-0.20	-0.22	0.06	0.04	0.74	1.05	1.42	-2.04
3.1	0.03	0.03	0.00	0.00	1.72	1.29	-0.80	-5.62
3.2	-0.14	-0.08	0.04	0.07	1.73	1.33	-1.99	-3.37

D. SYNTHETIC RESULTS FOR ALL THE TEST PERFORMED

For all the seventeen tests performed (see Table 1), the total distortion factor for harmonics (THD) and interharmonics ($TIHD$) have been calculated. Then, the percentage errors of the proposed model (M) for both AC absorbed current and

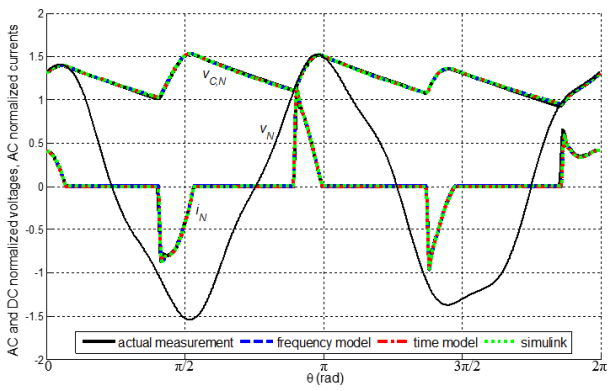

FIGURE 4. Test 3.1 (LED): AC supply voltage, v_N, AC absorbed current, i_N, and the DC-link voltage, $v_{C,N}$, waveforms obtained from actual measurement (solid black), frequency domain analytical model (dashed blue), time domain analytical model (dash-dotted red), and Simulink simulation (dotted green) versus the entire Fourier fundamental period.

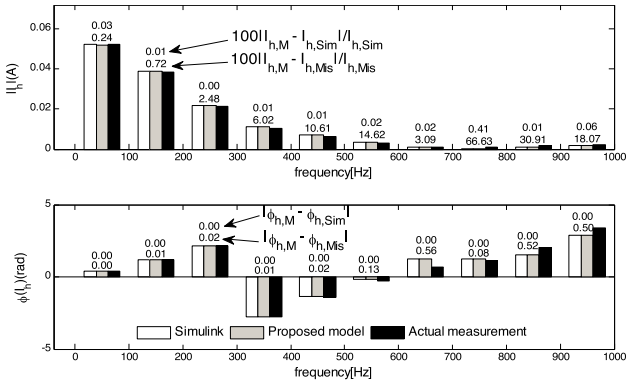

FIGURE 5. Test 3.1 (LED): AC absorbed current harmonics obtained from Simulink simulation, proposed model and actual measurement versus frequency.

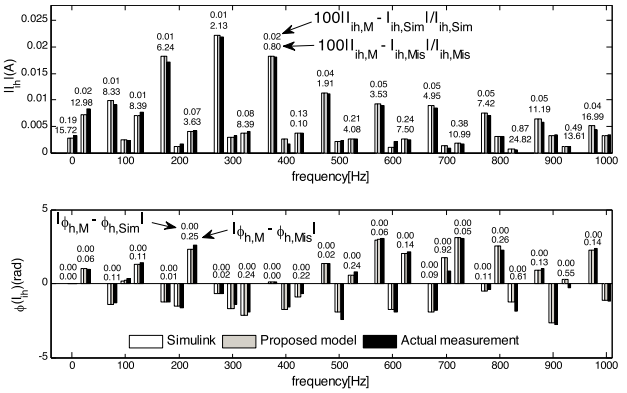

FIGURE 6. Test 3.1 (LED): AC absorbed current interharmonics obtained from Simulink simulation, proposed model and actual measurement versus frequency.

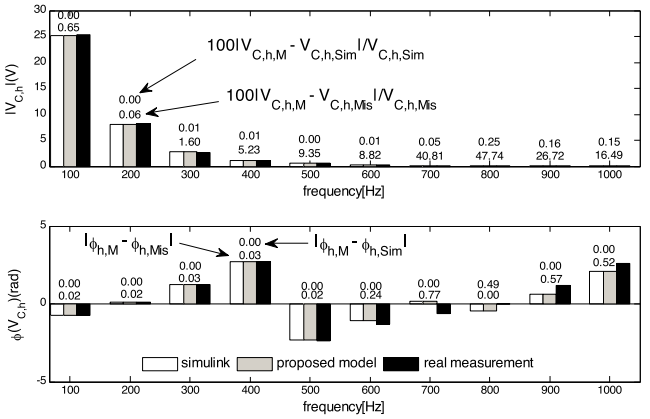

FIGURE 7. Test 3.1 (LED): DC-link voltage harmonics obtained from Simulink simulation, proposed model and actual measurement versus frequency.The DC component amplitude is 287.57 V for Simulink, 287.57 V for model and 286.89 V for the measurement; the corresponding errors of model-Simulink and model-measurement are respectively 0.00% and 0.24%.

DC-link voltage:

$$\varepsilon_{THD} = \frac{THD_M - THD_R}{THD_R} \cdot 100,$$
$$\varepsilon_{TIHD} = \frac{TIHD_M - TIHD_R}{TIHD_R} \cdot 100. \qquad (13)$$

are evaluated versus two different references R (*SIM* for Simulink simulations and *MIS* for actual measurements).

The percentage errors are reported in TABLE 3. It is possible to notice that their values are lower than 0.22%

$$\begin{pmatrix} C_k^{(j,1)} \\ G_k^{(j,1)} \end{pmatrix} = \frac{1}{s_1 - s_2} \begin{pmatrix} 1 \\ q \end{pmatrix} \left[\cos\delta_k \begin{pmatrix} -\beta_2 \\ s_1 + \beta_1 \end{pmatrix} + A(s_1) \begin{pmatrix} s_1 + \beta_3 \\ \beta_3 \end{pmatrix} \right], \quad \begin{pmatrix} C_k^{(j,2)} \\ G_k^{(j,2)} \end{pmatrix} = \frac{1}{s_2 - s_1} \begin{pmatrix} 1 \\ q \end{pmatrix} \left[\cos\delta_k \begin{pmatrix} -\beta_2 \\ s_2 + \beta_1 \end{pmatrix} + A(s_2) \begin{pmatrix} s_2 + \beta_3 \\ \beta_3 \end{pmatrix} \right]$$

$$\begin{pmatrix} C_k^{(j,3)} \\ G_k^{(j,3)} \end{pmatrix} = \begin{pmatrix} 1 \\ q \end{pmatrix} \left[-\frac{1}{s_1 - s_2} A(s_1) \begin{pmatrix} s_1 + \beta_3 \\ \beta_3 \end{pmatrix} - \frac{1}{s_2 - s_1} A(s_2) \begin{pmatrix} s_2 + \beta_3 \\ \beta_3 \end{pmatrix} \right],$$

$$\begin{pmatrix} C_k^{(j,4)} \\ G_k^{(j,4)} \end{pmatrix} = \frac{1}{s_1 s_2} \begin{pmatrix} 1 \\ q \end{pmatrix} \left[-\beta_2 \sin\delta_k \begin{pmatrix} \beta_3 \\ \beta_3 \end{pmatrix} + \frac{s_2 k}{s_1 - s_2} A(s_1) \begin{pmatrix} s_1 + \beta_3 \\ \beta_3 \end{pmatrix} + \frac{s_1 k}{s_2 - s_1} A(s_2) \begin{pmatrix} s_2 + \beta_3 \\ \beta_3 \end{pmatrix} \right],$$

$$G_k^{(j,0)} = \left[\left(G_k^{(j,1)} \right) e^{s_1(\theta_2^{(j)} - \theta_1^{(j)})} + \left(G_k^{(j,2)} \right) e^{s_2(\theta_2^{(j)} - \theta_1^{(j)})} + \left(G_k^{(j,3)} \right) \cos(k(\theta_2^{(j)} - \theta_1^{(j)})) + \left(G_k^{(j,4)} \right) \sin(k(\theta_2^{(j)} - \theta_1^{(j)})) \right], \quad (A.1)$$

when SIM results are assumed as reference and lower than 5.62% when MIS results are assumed as reference. As for the errors referred to actual measurement, it is important to observe that their magnitudes depend on the simplified circuit adopted and on the estimation of its parameters as discussed in Sub-section IV-B.

$$
\begin{aligned}
\underline{I}_{N,h}^{(j,1)} &= \frac{2}{\sqrt{2}}\frac{1}{2\pi}\int_{\theta_1^{(j)}}^{\theta_2^{(j)}} i_N^{(j,1)}(\theta)\cdot e^{-i\cdot h\theta}d\theta = \frac{1}{\pi}\sum_{k=1}^{K} V_{N,k}C_k^{(j,1)}\int_{\theta_1^{(j)}}^{\theta_2^{(j)}} e^{s_1(\theta-\theta_1^{(j)})}\cdot e^{-i\cdot h\theta}d\theta \\
&= H\sum_{k=1}^{K} V_{N,k}C_k^{(j,1)}\left(\frac{e^{s_1(\theta_2^{(j)}-\theta_1^{(j)})}\cdot e^{-i\cdot h\theta_2^{(j)}} - e^{-i\cdot h\theta_1^{(j)}}}{s_1 - i\cdot h}\right) \\
\underline{I}_{N,h}^{(j,2)} &= H\sum_{k=1}^{K} V_{N,k}C_k^{(j,2)}\left(\frac{e^{s_2(\theta_2^{(j)}-\theta_1^{(j)})}\cdot e^{-i\cdot h\theta_2^{(j)}} - e^{-i\cdot h\theta_1^{(j)}}}{s_2 - i\cdot h}\right) \\
\underline{I}_{N,h}^{(j,3)} &= H\left[\sum_{k=1;k\neq h}^{K} V_{N,k}C_k^{(j,3)}\left(\frac{e^{i((k-h)\theta_2^{(j)}-k\theta_1^{(j)})} - e^{-i\cdot h\theta_1^{(j)}}}{2i(k-h)} - \frac{e^{-i((k+h)\theta_2^{(j)}-k\theta_1^{(j)})} - e^{-i\cdot h\theta_1^{(j)}}}{2i(k+h)}\right)\right. \\
&\quad \left. + V_{N,h}C_h^{(j,3)}\left(\frac{(\theta_2^{(j)}-\theta_1^{(j)})e^{-i\cdot h\theta_1^{(j)}}}{2} - \frac{e^{-i(2h\theta_2^{(j)}-h\theta_1^{(j)})} - e^{-i\cdot h\theta_1^{(j)}}}{4i\cdot h}\right)\right] \\
\underline{I}_{N,h}^{(j,4)} &= H\left[\sum_{k=1;k\neq h}^{K} V_{N,k}C_k^{(j,4)}\left(\frac{e^{i((k-h)\theta_2^{(j)}-k\theta_1^{(j)})} - e^{-i\cdot h\theta_1^{(j)}}}{-2(k-h)} + \frac{e^{-i((k+h)\theta_2^{(j)}-k\theta_1^{(j)})} - e^{-i\cdot h\theta_1^{(j)}}}{-2(k+h)}\right)\right. \\
&\quad \left. + V_{N,h}C_h^{(j,4)}\left(\frac{(\theta_2^{(j)}-\theta_1^{(j)})e^{-i\cdot h\theta_1^{(j)}}}{2i} - \frac{e^{-i(2h\theta_2^{(j)}-h\theta_1^{(j)})} - e^{-i\cdot h\theta_1^{(j)}}}{4h}\right)\right] \\
&\quad \times \left(h = 0, 1, 2, 3, \ldots \text{ and } H = \sqrt{2}\Big/(2\pi) \text{ for } h = 0 \text{ or } H = 1/\pi \text{ for } h > 0\right).
\end{aligned}
\tag{B.1}
$$

$$
\begin{aligned}
\underline{V}_{C,N,m}^{(j,1)} &= M\sum_{k=1}^{K} V_{N,k}G_k^{(j,1)}\left(\frac{e^{s_1(\theta_2^{(j)}-\theta_1^{(j)})}\cdot e^{-i\cdot m\theta_2^{(j)}} - e^{-i\cdot m\theta_1^{(j)}}}{s_1 - i\cdot m}\right) \\
\underline{V}_{C,N,m}^{(j,2)} &= M\sum_{k=1}^{K} V_{N,k}G_k^{(j,2)}\left(\frac{e^{s_2(\theta_2^{(j)}-\theta_1^{(j)})}\cdot e^{-i\cdot m\theta_2^{(j)}} - e^{-i\cdot m\theta_1^{(j)}}}{s_2 - i\cdot m}\right) \\
\underline{V}_{C,N,m}^{(j,3)} &= M\left[\sum_{k=1;k\neq m}^{K} V_{N,k}G_k^{(j,3)}\left(\frac{e^{i((k-m)\theta_2^{(j)}-k\theta_1^{(j)})} - e^{-i\cdot m\theta_1^{(j)}}}{2i(k-m)} - \frac{e^{-i((k+m)\theta_2^{(j)}-k\theta_1^{(j)})} - e^{-i\cdot m\theta_1^{(j)}}}{2i(k+m)}\right)\right. \\
&\quad \left. + V_{N,m}G_m^{(j,3)}\left(\frac{(\theta_2^{(j)}-\theta_1^{(j)})e^{-i\cdot m\theta_1^{(j)}}}{2} - \frac{e^{-i(2m\theta_2^{(j)}-m\theta_1^{(j)})} - e^{-i\cdot m\theta_1^{(j)}}}{4i\cdot m}\right)\right] \\
\underline{V}_{C,N,m}^{(j,4)} &= M\left[\sum_{k=1;k\neq m}^{K} V_{N,k}G_k^{(j,4)}\left(\frac{e^{i((k-m)\theta_2^{(j)}-k\theta_1^{(j)})} - e^{-i\cdot m\theta_1^{(j)}}}{-2(k-m)} + \frac{e^{-i((k+m)\theta_2^{(j)}-m\theta_1^{(j)})} - e^{-i\cdot m\theta_1^{(j)}}}{-2(k+m)}\right)\right. \\
&\quad \left. + V_{N,m}G_m^{(j,4)}\left(\frac{(\theta_2^{(j)}-\theta_1^{(j)})e^{-i\cdot m\theta_1^{(j)}}}{2i} - \frac{e^{-i(2m\theta_2^{(j)}-m\theta_1^{(j)})} - e^{-i\cdot m\theta_1^{(j)}}}{4m}\right)\right] \\
\underline{V}_{C,N,m}^{(j,0)} &= M\sum_{k=1}^{K} V_{N,k}G_k^{(j,0)}\left(\frac{e^{-\beta_3(\theta_3^{(j)}-\theta_2^{(j)})}\cdot e^{-i\cdot m\theta_3^{(j)}} - e^{-i\cdot m\theta_2^{(j)}}}{-\beta_3 - i\cdot m}\right) \\
&\quad \times \left(m = 0, 1, 2, 3, \ldots \text{ and } M = \sqrt{2}\Big/(2\pi) \text{ for } m = 0 \text{ or } M = 1/\pi \text{ for } m > 0\right).
\end{aligned}
\tag{B.2}
$$

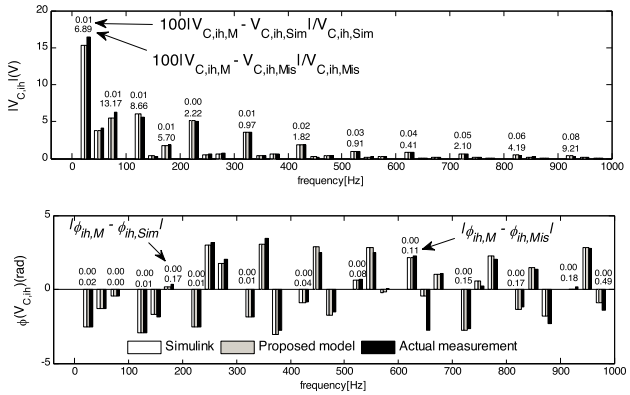

FIGURE 8. Test 3.1 (LED): DC-link voltage interharmonics obtained from Simulink simulation, proposed model and actual measurement versus frequency.

V. CONCLUSION

In this paper, a new accurate and comprehensive analytical model of harmonic and interharmonic distortion produced by a single-phase full-wave AC/DC diode rectifier is presented. Its main and new characteristic is the ability to consider the presence of interharmonics in addition to harmonics in the voltage at the terminals of the DBR based load due to the background voltage.

Analytical expressions able to predict DC voltage and AC current either in time or frequency domains have been developed. Several numerical and experimental tests have been performed on a "didactic" DBR load model and two DBR based lamps (CFL and LED), demonstrating very accurate results of the developed analytical model.

The proposed model presents all the advantages of analytical models (e.g., fastness); therefore, it can be easily integrated with iterative harmonic and interharmonic analysis procedures. Application of the model will give the possibility:

- to perform parametric analyses and probabilistic studies,
- to derive harmonically and interharmonically coupled admittance matrices to be included in harmonic and interharmonic power flow studies,
- to have a more direct insight in the physical behavior of the devices helping in introducing Standard limits for interharmonics.

The authors are working on the extension of the proposed modelling approach to three phase rectifiers.

APPENDIX A

The constants $C_k^{(j,i)}$ and $G_k^{(j,i)}$ (i=1 to 4 for $C_k^{(j,i)}$ and i=0 to 4 for $G_k^{(j,i)}$) in (6) are as in (A.1), shown at the bottom of page 7, where: $A(s) = \beta_2 \frac{s\cdot\cos(\delta_k^{(j)}) - k\cdot\sin(\delta_k^{(j)})}{k^2+s^2}$ and $\delta_k^{(j)} = k\theta_1^{(j)} + \phi_k$, with $s = s_1$ and $s = s_2$.

$$s_1 = a + b, \quad s_2 = a - b,$$
$$a = -\frac{\beta_1 + \beta_3}{2}, \quad b = \sqrt{\frac{(\beta_1 - \beta_3)^2}{4} - \beta_2\beta_3},$$
$$\beta_1 = \frac{r_N}{x_{L,N}}, \beta_2 = \frac{1}{x_{L,N}}, \beta_3 = x_{C,N}.$$

APPENDIX B

The phasor contributions obtained analytically applying the complex Fourier to each corresponding term in the expression (6) are as in (B.1) and (B.2), shown at the bottom of the previous page.

REFERENCES

[1] A. Mansoor, W. M. Grady, A. H. Chowdhury, and M. J. Samotyi, "An investigation of harmonics attenuation and diversity among distributed single-phase power electronic loads," *IEEE Trans. Power Del.*, vol. 10, no. 1, pp. 467–473, Jan. 1995.

[2] A. Mansoor, W. M. Grady, R. S. Thallam, M. T. Doyle, S. D. Krein, and M. J. Samotyj, "Effect of supply voltage harmonics on the input current of single-phase diode bridge rectifier loads," *IEEE Trans. Power Del.*, vol. 10, no. 3, pp. 1416–1422, Jul. 1995.

[3] A. Mansoor, W. M. Grady, P. T. Staats, R. S. Thallam, M. T. Doyle, and M. J. Samotyj, "Predicting the net harmonic currents produced by large numbers of distributed single-phase computer loads," *IEEE Trans. Power Del.*, vol. 10, no. 4, pp. 2001–2006, Oct. 1995.

[4] J. G. Mayordomo, L. F. Beites, R. Asensi, F. Orzaez, M. Izzeddine, and L. Zabala, "A contribution for modeling controlled and uncontrolled AC/DC converters in harmonic power flows," *IEEE Trans. Power Del.*, vol. 13, no. 4, pp. 1501–1508, Oct. 1998.

[5] G. Carpinelli, F. Iacovone, P. Varilone, and P. Verde, "Single phase voltage source converters: Analytical modeling for harmonic analysis in continuous and discontinuous current conditions," *Int. J. Power Energy Syst.*, vol. 23, no. 1, pp. 37–48, 2003.

[6] L. Sainz, J. J. Mesas, and A. Ferrer, "Characterization of non-linear load behavior," *Electr. Power Syst. Res.*, vol. 78, no. 10, pp. 1773–1783, Oct. 2008.

[7] J. Yong, L. Chen, A. B. Nassif, and W. Xu, "A frequency-domain harmonic model," *IEEE Trans. Power Del.*, vol. 25, no. 2, pp. 1182–1189, Apr. 2010.

[8] J. G. Mayordomo, A. Carbonero, L. F. Beites, and W. Xu, "Decoupled Newton algorithms in the harmonic domain for the harmonic interaction of line commutated converters with AC systems," *IEEE Trans. Power Del.*, vol. 25, no. 3, pp. 1721–1733, Jul. 2010.

[9] J. Yong, L. Chen, A. B. Nassif, and W. Xu, "A frequency-domain harmonic model for compact fluorescent lamps," *IEEE Trans. Power Del.*, vol. 25, no. 2, pp. 1182–1189, Apr. 2010.

[10] J. J. Mesas, L. Sainz, and J. Molina, "Parameter estimation procedure for models of single-phase uncontrolled rectifiers," *IEEE Trans. Power Del.*, vol. 26, no. 3, pp. 1911–1919, Jul. 2011.

[11] J. Yong, L. Chen, and S. Chen, "Modeling of home appliances for power distribution system harmonic analysis," *IEEE Trans. Power Del.*, vol. 25, no. 4, pp. 3147–3155, Oct. 2010.

[12] R. Senra, W. C. Boaventura, and E. M. A. M. Mendes, "Assessment of the harmonic currents generated by single-phase nonlinear loads," *Electr. Power Syst. Res.*, vol. 147, pp. 272–279, Jun. 2017.

[13] M. Wcislik, "Analytical model of single-phase AC circuit with inductance and bridge rectifier," *Przegląd Elektrotechniczny*, vol. 1, pp. 128–131, Jan. 2018.

[14] L. F. Beites, J. G. Mayordomo, and X. Yang, "The harmonically coupled admittance matrix of the single-phase diode rectifier," *IEEE Access*, vol. 9, pp. 128023–128031, 2021, doi: 10.1109/ACCESS.2021.3110597.

[15] A. Testa et al., "Interharmonics: Theory and modeling," *IEEE Trans. Power Del.*, vol. 22, no. 4, pp. 2335–2348, Oct. 2007.

[16] R. Carbone, D. Menniti, R. E. Morrison, and A. Testa, "Harmonic and interharmonic distortion modeling in multiconverter systems," *IEEE Trans. Power Del.*, vol. 10, no. 3, pp. 1685–1692, Jul. 1995.

[17] R. Carbone, F. DeRosa, R. Langella, and A. Testa, "A new approach for the computation of harmonics and interharmonics produced by line-commutated AC/DC/AC converters," *IEEE Trans. Power Del.*, vol. 20, no. 3, pp. 2227–2234, Jul. 2005.

[18] F. D. Rosa, R. Langella, A. Sollazzo, and A. Testa, "On the interharmonic components generated by adjustable speed drives," *IEEE Trans. Power Del.*, vol. 20, no. 4, pp. 2535–2543, Oct. 2005.

[19] G. W. Chang and S. K. Chen, "An analytical approach for characterizing harmonic and interharmonic currents generated by VSI-fed adjustable speed drives," *IEEE Trans. Power Del.*, vol. 20, no. 4, pp. 2585–2593, Oct. 2005.
[20] R. Langella, A. Sollazzo, and A. Testa, "A new approach for the computation of harmonics and interharmonics produced by AC/DC/AC conversion systems with PWM inverters," *Eur. Trans. Electr. Power*, vol. 20, no. 1, pp. 68–82, Jan. 2010.
[21] S. Tennakoon, S. Perera, and D. Robinson, "Flicker attenuation—Part I: Response of three-phase induction motors to regular voltage fluctuations," *IEEE Trans. Power Del.*, vol. 23, no. 2, pp. 1207–1214, Apr. 2008.
[22] A. Ramirez, "The modified harmonic domain: Interharmonics," *IEEE Trans. Power Del.*, vol. 26, no. 1, pp. 235–241, Jan. 2011.
[23] G. W. Chang, S.-K. Chen, H.-J. Su, and P.-K. Wang, "Accurate assessment of harmonic and interharmonic currents generated by VSI-fed drives under unbalanced supply voltages," *IEEE Trans. Power Del.*, vol. 26, no. 2, pp. 1083–1091, Apr. 2011.
[24] L. Feola, R. Langella, and A. Testa, "On the effects of unbalances, harmonics and interharmonics on PLL systems," *IEEE Trans. Instrum. Meas.*, vol. 62, no. 9, pp. 2399–2409, Sep. 2013.
[25] R. Langella, A. Testa, J. Meyer, F. Moller, R. Stiegler, and S. Z. Djokic, "Experimental-based evaluation of PV inverter harmonic and interharmonic distortion due to different operating conditions," *IEEE Trans. Instrum. Meas.*, vol. 65, no. 10, pp. 2221–2233, Oct. 2016.
[26] J. Drapela et al., "Issues and challenges related to interharmonic distortion limits," in *Proc. 19th Int. Conf. Harmon. Quality Power (ICHQP)*, Jul. 2020, pp. 1–6, doi: 10.1109/ICHQP46026.2020.9177933.
[27] *IEEE Standard for Harmonic Control in Electric Power Systems*, Standard 519–2022 (Revision of IEEE Std 519-2014), Aug. 2022, pp. 1–31, doi: 10.1109/IEEESTD.2022.9848440.
[28] R. Langella, A. Testa, V. Vendemia, and J. Drapela, "New comprehensive analytical model of single-phase AC/DC diode rectifiers in the presence of interharmonics in supply voltage," in *Proc. 20th Int. Conf. Harmon. Quality Power (ICHQP)*, May 2022, pp. 1–6, doi: 10.1109/ICHQP53011.2022.9808466.
[29] J. Drapela, R. Langella, J. Slezingr, and A. Testa, "Generalized lamp model for light flicker studies," *Electric Power Syst. Res.*, vol. 154, pp. 413–422, Jan. 2018, doi: 10.1016/j.epsr.2017.09.007.
[30] J. Molina and L. Sainz, "Model of electronic ballast compact fluorescent lamps," *IEEE Trans. Power Del.*, vol. 29, no. 3, pp. 1363–1371, Jun. 2014.
[31] J. Drapela and J. Slezingr, "Flickering of lamps due to ripple control signal," in *Proc. IEEE Trondheim PowerTech*, Jun. 2011, pp. 1–7.

JIRI DRAPELA (Senior Member, IEEE) received the M.Sc. and Ph.D. degrees in electrical power engineering from the Brno University of Technology, Brno, Czech Republic, in 1999 and 2006, respectively. He is currently with the Brno University of Technology as a Full Professor of power systems and the Team Leader of the Power Quality Research Group. His research interests include power quality and power network conducted disturbances, especially immunity, emission of electrical appliances, and power quality measurement techniques.

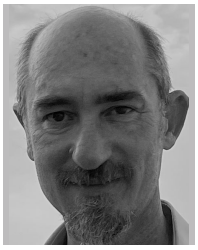

ROBERTO LANGELLA (Senior Member, IEEE) was born in Naples, Italy, in March 1972. He received the Laurea degree in electrical engineering from the University of Naples, Italy, in 1996, and the Ph.D. degree in electrical energy conversion from the University of Campania "Luigi Vanvitelli," Italy, in 2000. He is currently a Full Professor of electrical power systems with the University of Campania "Luigi Vanvitelli." He is the Chair of the IEEE PES TF on Harmonic Modeling, Simulation, and Assessment.

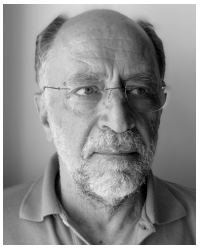

ALFREDO TESTA (Life Fellow, IEEE) was born in Naples, Italy, in March 1950. He received the Laurea degree in electrical engineering from the University of Naples Federico II, Naples, in 1975. He is currently an Emeritus Professor with the University of Campania "Luigi Vanvitelli," Aversa, Italy. His research interests include electrical power systems reliability and harmonic analysis.

VINCENZO VENDEMIA was born in Caserta, Italy, in November 1989. He received the bachelor's degree in electronic engineering and the master's degree in power electronics engineering from the University of Campania "Luigi Vanvitelli" in 2012 and 2017, respectively. He is currently a Power Electronics Engineer with NIDEC ASI S.p.A.

Open Access funding provided by 'Università degli Studi della Campania "Luigi Vanvitelli"' within the CRUI CARE Agreement